Journal of Materials Chemistry A

Energetic decomposition yields efficient bimetallic Cu MOF-derived catalysts

Journal:	*Journal of Materials Chemistry A*
Manuscript ID	TA-ART-05-2020-004765.R1
Article Type:	Paper
Date Submitted by the Author:	30-Jun-2020
Complete List of Authors:	Nguyen-Sorenson, Anh ; Brigham Young University, Chemistry and Biochemistry Wu, Yu; Sichuan University of Science and Engineering Orcutt, Emma; Brigham Young University Kent, Rosalyn; University of Michigan, Chemistry Anderson, Hans; Brigham Young University, Chemistry and Biochemistry Matzger, Adam; University of Michigan, Chemistry Stowers, Kara; Brigham Young University, Chemistry and Biochemistry

SCHOLARONE™
Manuscripts

ARTICLE

Energetic decomposition yields efficient bimetallic Cu MOF-derived catalysts

Received 00th January 20xx,
Accepted 00th January 20xx

DOI: 10.1039/x0xx00000x

Anh H. T. Nguyen Sorenson,[a] Yu Wu,[c] Emma K. Orcutt,[a] Rosalyn V. Kent,[b] Hans C. Anderson,[a] Adam J. Matzger,[b] and Kara J. Stowers*[a]

Metal-organic frameworks (MOFs) have recently emerged as efficient self-sacrificial templates to fabricate porous carbon-supported metal nanoparticles (NPs). Due to observed increased activity, catalysts containing bimetallic NPs represent an active frontier for heterogeneous catalyst development. A strategy to synthesize active catalysts with highly dispersed bimetallic metal/metal oxides within a porous carbon matrix via rapid MOF decomposition using dopants is presented in this paper. A 2,4,6-trinitrotoluene (TNT) additive enhances the rapid thermolysis of the metal-doped Cu-based MOFs to minimize particle aggregation. Catalyst characterization reveals that a secondary metal increases dispersion of both metals over the carbon composite support. The catalyst preparation method influences both the metal particle size and oxidation state. Catalytic performance shows increased rates for 4-nitrophenol reduction even with <1 wt% of added secondary metal. Among the synthesized catalysts, the Ni-CuO@C bimetallic catalyst exhibits outstanding activity. This synthetic strategy is useful for creating highly efficient, robust, non-noble metal catalysts for development of sustainable chemical processes.

Introduction

Metal-organic frameworks (MOFs) are a rapidly developing class of porous materials due to their high surface areas, ordered structures, and tunable functionality.[1-4] Recently, there is increasing study toward using MOFs as catalysts,[5] gas storage and separation materials,[6] drug delivery agents,[7] and chemical sensors.[8,9] In addition to these applications, approaches to use MOFs as sacrificial templates to develop carbon supported nanoparticles (NPs) and apply them as heterogeneous catalysts has gained traction.[10,11]

From multiple perspectives, Cu-based catalysts are great candidates for small molecule redox reactions due to their accessible oxidation states, abundance and non-toxicity. An important catalytic reduction is of nitro-aromatic compounds, that are highly hazardous to the environment and potentially toxic toward humans, animals, and plants.[12-14] It is highly desirable to reduce these to more useful groups. Anilines serve as intermediates and precursors in the synthesis of a variety of fine chemicals.[15] For example, while 4-nitrophenol is a waste product of pesticides and dye production, the reduced 4-aminophenol is an intermediate in the synthesis of paracetamol.[16,17] The hydrogenation of 4-nitrophenol (4-NP) to 4-aminophenol (4-AP) is a model reaction within this reaction class to evaluate and benchmark catalytic performance.[18,19]

Although Cu-based catalysts are active for this reduction class, a second metal will often boost the catalytic performance of monometallic catalysts by modifying the structure and electronic effects. Often this additional metal increases uniformity with respect to particle size and shape which results in better control of activity and/or substrate selectivity.[20,21] The thermolysis of bimetallic Cu-based MOFs with a molar 2:1 ratio of Cu:Ni had excellent performance in catalytic oxidation of furfural to cyclopentanone.[20] The addition of Ni increased uniform dispersion to obtain an average particle size of about 15 nm and Cu particles were reduced more easily. A bimetallic Cu-based MOF with a molar 5:2 ratio of Cu:Co also had better dispersion of the Co and Cu with uniform oxidation states after thermolysis.[21]

Due to the wide variety of building blocks available, the sacrificial MOF template can be tuned for design of porous carbon materials obtained under thermolysis conditions.[22-26] Previously, we have shown that the unique and high energy CuNbO-1 MOF transforms into an amorphous copper and anisotropic carbon nanocomposite, a-Cu@C, with finely dispersed copper NPs throughout the layers of an anisotropic carbon structure.[27] This catalyst performs well as a heterogeneous catalyst for oxidation of benzyl alcohol, reduction of nitrobenzene, and N-arylation.[28] The exceptional properties of this catalyst are ascribed to its unusual deflagrative method of synthesis, wherein rapid decomposition creates only transient high temperatures allowing kinetic trapping of highly active nanoparticles upon cooling; this method contrasts with the ubiquitous high temperature annealing approach.

[a] Department of Chemistry and Biochemistry Department, Brigham Young University, Provo, Utah, 84604, USA. E-mail: kstowers@chem.byu.edu
[b] Department of Chemistry and Macromolecular Science and Engineering Program, University of Michigan, 930 North University Ave, Ann Arbor, Michigan 48109-1055, USA.
[c] College of Chemistry and Environmental Engineering, Sichuan University of Science & Engineering, Zigong, 643000, P. R. China.

† Electronic Supplementary Information (ESI) available. See DOI: 10.1039/x0xx00000x

In the present study, we target bimetallic Cu-based catalysts and increased activity from the interactions between two metals. The bimetallic Cu-based catalysts (M-CuO@C with M = Ni, Co, Ag) are fabricated by one-step thermal decomposition of a metal-doped copper containing MOF HKUST-1 (Cu-BTC, BTC = 1,3,5-benzene tricarboxylate) with the explosive 2,4,6-trinitrotoluene (TNT) as an additive. The addition of an available highly energetic dopant aids initiation of a rapid thermolysis, in much the same way CuNbO-1 does, with the considerable advantage that commercially available Cu-BTC can be used as the sacrificial MOF. Here we report the catalytic activity of the synthesized catalysts and characterize the interaction of M-CuO via the kinetic study of the reduction of 4-NP to 4-AP with $NaBH_4$ as a hydride source at room temperature. The influence of a secondary metal is investigated with respect to particle size, reaction time, turnover rate and rate constant.

Experimental

Materials

All reagents and starting materials were purchased commercially from Sigma-Aldrich or Alfa-Aesar and used as received without any further purification unless otherwise noted.

Synthesis and activation of HKUST-1

Synthesis of HKUST-1 was performed according to reported literature methods with details give in the supporting information.[29]

Synthesis of HKUST-1/TNT (CuO@C)

Activated HKUST-1 crystals (25 mg) and TNT (50 mg) were added to a 4 mL vial in the glove box and shaken for 5 minutes. The vial was removed from the glovebox and then heated at 90 °C for 2 h. The explosive mixture was then carefully transferred to a copper pan and sealed before thermal initiation. A torch was then used to pre-heat the sealed end. Once heated for a few seconds, the copper pan was knocked into the hot region and thermally initiated. CuO@C was captured in an Erlenmeyer flask at the open end of the tube and collected for analysis. See Supporting Information for more details.

Synthesis of HKUST-1/TNT/M (M-CuO@C)

Activated HKUST-1 crystals (800 mg) and M salt (typically the nitrate) were added to a 20 mL glass vial in a nitrogen filled glovebox. The vial was shaken by hand and then removed and methanol (1.5 mL) was added to the mixture and then shaken again. Finally, the suspension was placed in a shaker at room temperature for 7 days. See Supporting Information for more details. Methanol was then evaporated by a slow stream of air flowing over the uncapped vial for 2h. The solid doped M/HKUST-1 composite was collected. M/HKUST-1 (25 mg) and TNT (50 mg) were added to a 4 mL vial in the glove box. The vial was removed from the glovebox and then heated at 90 °C for 2 h. The explosive mixture was then carefully transferred to a copper pan and sealed. Finally, M-CuO@C was produced by the thermolysis procedure detailed above. The Cu wt% loading and M (M = Ni, Co, and Ag) wt% loading was determined by inductively coupled plasma optical emission spectrometry from Perkin-Elmer Optima (8300 ICP-OES) using argon and a collision cell filled with ultra-high-purity helium both from Airgas. Silver, nickel and cobalt doped M-CuO@C are designated as Ag-CuO@C, Ni-CuO@C and Co-CuO@C with further details in the supporting information.

Characterization of M-CuO@C

XRD Powder patterns were collected with a Panalytical Empyrean using Cu-Kα radiation (λ = 1.54187 Å) and operating at 45 kV and 40 mA. Samples were prepared by pressing them onto a glass slide fitted into a sample holder to minimize height error. Gas Sorption experiments were carried out using a NOVA surface area analyzer (Quantachrome Instruments, Boynton Beach, Florida, USA). Raman spectra were collected using a Renishaw inVia Raman Microscope in extended scan mode with a range of 2500-100 cm^{-1}. Scanning transmission electron microscopy-energy dispersive X-ray spectroscopy (STEM-EDX) and TEM studies were performed on a Tecnai F20 TEM using an accelerating voltage of 200 kV. X-ray photoelectron spectroscopy (XPS) was performed using a Surface Science SSX-100 XPS instrument (Service Physics, Bend, OR) with a monochromatic Al Kα source (1486.7 eV) and a hemispherical analyzer.

Reduction of 4-Nitrophenol – UV-Vis Studies and Batch Reactions

The kinetic studies were performed on an Agilent 8453 G1103A Spectrophotometer. In a typical experiment, catalyst (1 mg) was measured and transferred into a 100 mL beaker containing D.I. water (56 mL) and a stir bar. Under vigorous stirring, sodium borohydride solution (10 mL) was added to reaction with the kinetic run was starting immediately. Aliquots were withdrawn and diluted prior to taking UV-Vis spectra. Spectra were collected in the range of 200-900 nm every 50 seconds until the reaction reached completion. The corresponding amine products were confirmed by the GC-MS. For a typical batch reaction, nitrobenzene and THF:H_2O solution were added, followed by the addition of catalyst (0.01-0.05 mmol Cu loading) to the mixture. $NaBH_4$ dissolved in D.I. H_2O was then added to the reaction mixture under vigorous stirring. The mixture was stirred for 2 h at 70 °C. Once the reaction was completed, it was cooled to room temperature prior to workup. A yield of aniline product was determined by integration using an internal standard biphenyl in the GC-MS. Catalyst leaching was confirmed by ICP-OES.

Results and Discussion

Characterization of CuO@C and M-CuO@C (M = Ni, Co, Ag)

During the pyrolysis process, the organic ligands in a MOF play two important roles: acting as a reductant to reduce framework

This journal is © The Royal Society of Chemistry 20xx

Please do not adjust margins

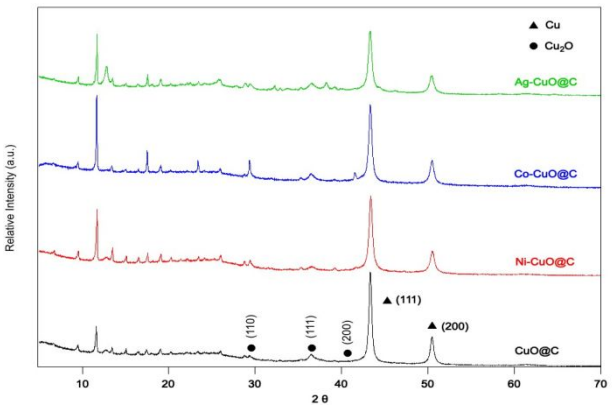

Fig. 1 PXRD spectra of CuO@C (black), Ni-CuO@C (red), Co-CuO@C (blue) and Ag-CuO@C (green).

metal ions[30] and to act as a precursor of the porous carbon matrix.[31] Because Cu^{2+} ions have a reduction potential higher than -0.27 V, the reduced metal nanoparticle is formed through reduction from the carbon of the ligands. This synthetic strategy thus obviates further post-reduction synthetic steps. The TNT additive acts to rapidly initiate thermolysis and consequently may result in a small amount of Cu^{2+} left as oxidized Cu_2O. The particle sizes and crystallinity of the products were characterized by powder X-ray diffraction (PXRD). The PXRD patterns of all decomposed catalysts show the copper metallic phase and copper oxide phase peaks (Fig. 1). Diffraction peaks at 2θ = 43.5° and 50.6° are ascribed to the (111) and (200) crystal planes of metallic Cu nanoparticles (JCPDS NO. 85-1326).[32] The Cu_2O nanoparticle peaks are at 2θ = 29°, 36.5°, and 41.5°, assigned to the (110), (111), and (200) crystal planes (JCPDS NO. 78-2076).[33] These diffraction patterns confirm that the derived catalysts primarily contain metallic Cu nanoparticles in the cubic structure.

In the bimetallic M-CuO@C (M = Ni, Co, and Ag) catalyst PXRD patterns, no obvious secondary metal peaks are detected. This suggests a fine distribution of < 3 nm nanoparticles or amorphous secondary metal species phase. Comparing the width of 2θ = 43.5° and 50.6° peaks in the bimetallic catalysts to the CuO@C catalyst slight increases indicate that bimetallic addition has yielded smaller Cu crystallites. This may be due to partial secondary metal ion substitution for cupric ions in the HKUST-1 framework and/or the secondary metal ions within HKUST-1 channels.[34] Both would lead to minimized aggregation of copper ions during framework decomposition.

The average crystallite domain sizes were calculated by the Debye-Scherrer equation (Supporting Information, Table S1). The synthesized CuO@C catalyst has crystallite sizes of 18.5 nm. The addition of a secondary metal yielded an average of domain size of 13±1 nm. Similar observations of a decrease in size with addition of a secondary metal were obtained by Wang's group.[20,21] The PXRD patterns of the derived catalysts also show a few characteristic peaks of the original HKUST-1 and this likely results from ejection of solids during the violent deflagration process. Thus, the synthesized catalysts retain some porous character after thermal treatment (Supporting Information, Fig. S2).[35,36]

The metal component ratios, loadings, and the derived-catalyst surface areas are tabulated in Table 1. According to

Table 1 Surface and physical properties of all the Cu-based catalysts.

Catalyst	Cu (wt%)	M (wt%)	Total metal (wt%)	SA ($m^2 \cdot g^{-1}$)
CuO@C	26.7	---	26.7	9.0
Ni-CuO@C	24.8	0.8	25.5	9.4
Co-CuO@C	26.7	0.9	27.6	10.3
Ag-CuO@C	26.1	0.6	26.7	12.9

ICP-OES analysis, the catalysts have around 25 – 27 wt% Cu. The Cu loading of Ni-CuO@C has slightly less Cu compared to the non-bimetallic and other bimetallic catalysts.

The sample pore structure and surface area were investigated using N_2 adsorption-desorption isotherms and all showed similar characteristics as shown for CuO@C in Fig. 2. The isotherms of all samples are type II, which is characteristic of diameters larger than a micropore or ~ 2 nm.[37] (The other isotherms are found in the supporting information Fig. S3). From the BET analysis of N_2 adsorption-desorption isotherms, all catalysts exhibit a surface area of ~ 9.0 – 12.9 m^2/g (Table 1). This small surface area results from particle agglomeration, pore blockage, or collapse. The surface area increases only slightly with addition of a second metal in the order of Ni < Co < Ag with 12.9 m^2/g as the largest surface area obtained. The porous structure of CuO@C and bimetallic M-CuO@C catalysts is composed of micro-, meso- and macro-pores therefore metal species can be dispersed both on the internal and external surface of the carbon matrix. The distinct increase in adsorbate volume in the low P/P_0 region (below 0.4) indicates the presence of micropores, which are residual from the porous structure in the samples (see PXRD spectra).[38] The hysteresis loop at P/P_0 = 0.4 – 0.6, indicative of mesopores, has very small N_2 uptake, suggesting only a small concentration of these pores. The strong N_2 uptake at P/P_0 above 0.6 confirms that the surface of catalysts is mainly macropores.[39]

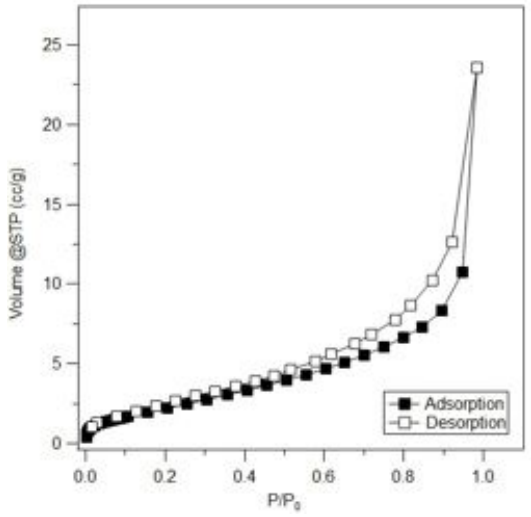

Fig. 2 N_2 adsorption-desorption isotherm for CuO@C.

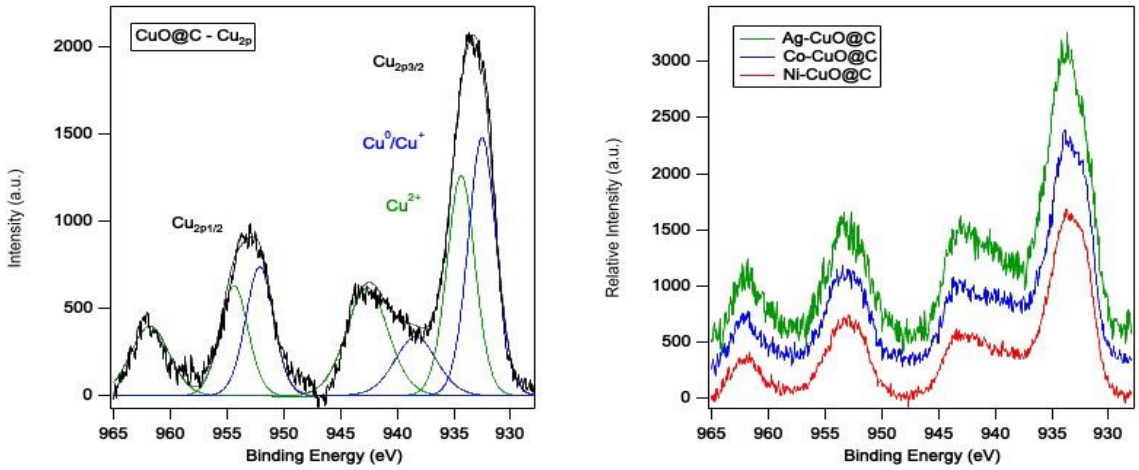

Fig. 3 XPS spectra of Cu 2p from CuO@C (left, black), Ni-CuO@C (red), Co-CuO@C (blue) and Ag-CuO@C (green).

The chemical composition of the derived catalysts was also studied by XPS analysis as shown in Fig. 3. While under N_2 conditions, the decomposition of HKUST-1 primarily shows reduced Cu species, in our sample there is a mixture of Cu^+ and Cu^{2+} species. The decomposed benzoate ligands lead to Cu^{2+} reduction.[40] However, the presence of oxidized states can be from the highly oxidizing power of the TNT additive with residual surface oxidation of the samples from air and moisture exposure.

For all of the samples, the main peaks for Cu $2p_{3/2}$ at ~932 eV and ~934 eV are ascribed to $Cu^{0/+}$ and Cu^{2+} respectively.[41-43] The majority of the C 1s spectrum is sp^2-carbon with graphitic nature (Supporting information, Fig. S4).[44] There is also evidence of copper and/or secondary metal coordinated N, graphitic N and oxidized N originating from the TNT (Supporting information, Fig. S5).[45-47] The O 1s spectrum shows evidence for M-O, M-OH and oxidized carbon (Supporting information, Fig. S7). The peak at ~530.4 eV is associated with M–O and M–OH groups, while those at 533 and 535 eV are related to C–OH and C=O groups.[48]

With <1wt% addition of the second metal, it is difficult to observe the XPS signal (Supporting information, Fig. S6). In the Ni-CuO@C sample, the doublet Ni $2p_{3/2}$ peak at 854.8 eV and Ni $2p_{1/2}$ peak at 872 eV can be assigned to Ni(II).[49] No evidence of Ni^0 is present which is predicted by redox potentials.[30] The Ag 3d signal in the Ag-CuO@C spectra has a doublet at 367.1 eV which can be ascribed to Ag(I).[38] Surprisingly, there are no XPS peaks associated with Co species found in Co-CuO@C catalyst. This suggests that Co nanoparticles are likely to be dispersed in the pores or encapsulated by carbon.

The Raman spectra for all of the synthesized catalysts, (Supporting Information, Fig. S8) show two broad bands at ~1579 cm^{-1} and 1352 cm^{-1} corresponding to the G (E_{2g}) and D (A_{1g}) breathing modes, respectively.[50] The significant D mode confirms structural defects and disorders in the carbon matrix of materials, while the G mode associates with sp^2 carbon domains.[51-53]

In order to examine the morphology of the catalysts, particle distribution, and size, analysis was performed with STEM and TEM as shown in Fig. 4 (Supporting information, Fig. S9-12). The catalysts exhibit sponge-like porous structures with dispersed spherical nanoparticle species. The CuO@C catalyst has finely distributed particles with an average particle size of about 27.0 ± 6.8 nm both on the surface and within the pores (Fig 4a). There is a somewhat broad distribution of particles but the majority are ~ 22-26 nm (Fig. 4e). The higher average particle sizes obtained from STEM and TEM analysis compared to PXRD are due to closely overlapping particles. The interplanar spacings of metallic Cu (111) and Cu (200) correspond to the lattice fringes (0.22 and 0.18 nm spacing) that can be seen in HRTEM and confirmed with analysis of the selected-area electron diffraction (SAED) pattern (Fig. S9). The diffraction rings result only from Cu which is consistent all amorphous carbon composite as observed in the Raman spectra.

Dispersed metal particles are observed both on the surface and within the pores of the carbon composite in the STEM/TEM of the bimetallic catalysts M-CuO@C in Fig. 4b-d (Supporting information, Fig. S10-12). The same lattice spacing for Cu(111) and Cu(200) are present in the M-Cu catalyst with an additional Cu(311) plane observed. Overall, particles sizes and distributions for M-CuO@C catalysts confirm that Cu has increased dispersion with added metals to HKUST-1 prior to decomposition. A comparison yields that the Ni-CuO@C catalyst exhibits a more homogeneous particle distribution, whereas the Co- and Ag-CuO@C have a bimodal distribution of particle sizes.

The average particle size for Ni-CuO@C is 18.6 ± 4.8 nm (Fig. 4b and f), which agrees with the PXRD smaller particle size for the bimetallic catalyst. Analysis of SAED in Ni-CuO@C and Co-CuO@C also show that the Ni(220) and Co(221) planes are present. The particle size distribution for Ag-CuO@C, 6.6 ± 1.7 nm and 22.3 ± 3.1 nm (Fig. 4d and h). The Ag-CuO@C catalyst displays the most sponge-like structure of the three with minimal to no Ag detected on Cu particles according to EDX analysis (Fig. S12) as well as over larger regions likely caused from low Ag loading (0.55 wt%). Two particle sizes are present in Co-CuO@C; 6.1 ± 3.8 nm and 45.5 ± 7.0 nm (Fig. 4c and g). The large particles may consist of aggregates of small nanoparticles encapsulated in carbon. These types of encapsulated aggregates are consistent with previously published copper[28] and cobalt[54] MOF decomposition materials.

This journal is © The Royal Society of Chemistry 20xx

Please do not adjust margins

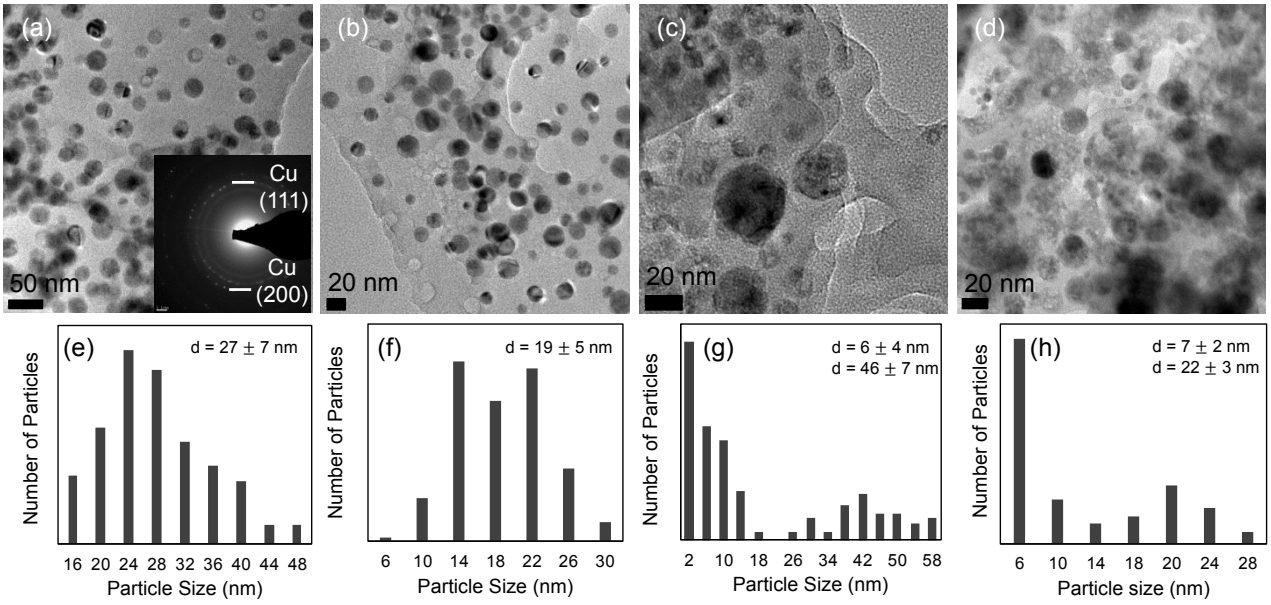

Fig. 4 TEM images of (a) CuO@C with 50 nm scale bar with an inset of electron diffraction patterns and of M-CuO@C catalysts where M is (b) Ni, (c) Co, and (d) Ag with 20 nm scale bar. Particle histogram of (e) CuO@C and of M-CuO@C where M is (f) Ni, (g) Co, and (h) Ag.

Analysis with scanning transmission electron microscopy-energy dispersive X-ray spectroscopy (STEM-EDS) and diffraction patterns from transmission electron microscopy (TEM) images (Fig. S11) confirms the small particles to be Co species with small amounts of Co bound to Cu particles. No distribution of Co is seen on the external surface of carbon, which is consistent with XPS results.

Kinetic studies of 4-nitrophenol reduction

The catalysts (CuO@C and M-CuO@C with M = Ni, Co, Ag) were compared for the reduction of 4-nitrophenol (4-NP) to 4-aminophenol (4-AP) as a model reaction.[19] Without a catalyst, the UV-Vis absorption spectra of 4-NP remained unchanged and with $NaBH_4$ added the absorption peak of 4-NP was red-shifted as the 4-nitrophenolate species (Fig. 5a).[55,56] When CuO@C was added, the absorption intensity of 4-NP decreased while the absorption peak of 4-AP increased showing a clear isosbestic point between the two peaks indicating no observable side products (Fig. 5b).[33] After addition of the catalysts, the reduction reaction started immediately without any induction period (Fig. S13).[55]

The analysis of the reduction of 4-NP was carried out with a large excess of borohydride in order to make the reaction independent of the borohydride concentration (100:1 mol% $NaBH_4$:4-NP) and fitted reasonably well to nearly 100% of the conversion of the reactions (Fig. 5c). The calculated turnover frequencies, rate constants (*k*) and activity factors (K) were used to compare the catalytic activity of the bimetallic catalysts synthesized here with similar catalysts. The activity factors, K, were calculated as the ratio of the rate constant (*k*) over the total weight of the catalyst.

The CuO@C catalyzed reaction reached completion (>99 % conversion) within 6.7 min, whereas M-CuO@C catalyzed reactions reached the same conversion at shorter times (Fig 5b, Fig. S14). However, Ag-CuO@C (0.876 min^{-1} completed at 5.0 min) performed only slightly better than the original CuO@C (0.804 min^{-1} completed at 6.7 min). This could be due to the low wt% Ag in the catalyst or also that Ag has little to no inherent reduction properties. Both Co-CuO@C and Ni-CuO@C showed higher activity than Cu alone. NiCuO@C reduced 4-NP to 4-AP with >99 % conversion within 3.3 min (k = 1.578 min^{-1}) resulting in a turnover frequency of 12 mmol/g_{cat}/min. A low wt% loading of nickel almost doubles activity. The Ni-CuO@C catalyst also has the least amount of Cu compared to the other catalysts. This increase in activity would be consistent with a modified surface electronic structure of the bimetallic catalyst compared to the corresponding Cu catalyst alone. This electronic change may facilitate the formation of the required surface intermediate that allows for better hydride dispersion from the $NaBH_4$ or influences the binding strength between the active metal species and the phenolate intermediate. Electron transfer would then occur following the Langmuir-Hinshelwood mechanism.[56] A known shifting of the d-band of the bimetallic surface to between the d-band for Cu and Ni alone may consequently result in not too weak and not too strong binding energy for adsorption of 4-NP and release of 4-AP which results in enhanced reduction. This increased activity was found for a NiCu catalyst used for ammonia borane hydrolysis.[57,58] These results contrast with usual observations that higher catalyst surface area leads to better activity; the activity enhancement of Ni suggests that the smaller and more homogeneous Cu particle size in the Ni-CuO@C leads to higher active site concentration for contact with the reactants.

This journal is © The Royal Society of Chemistry 20xx

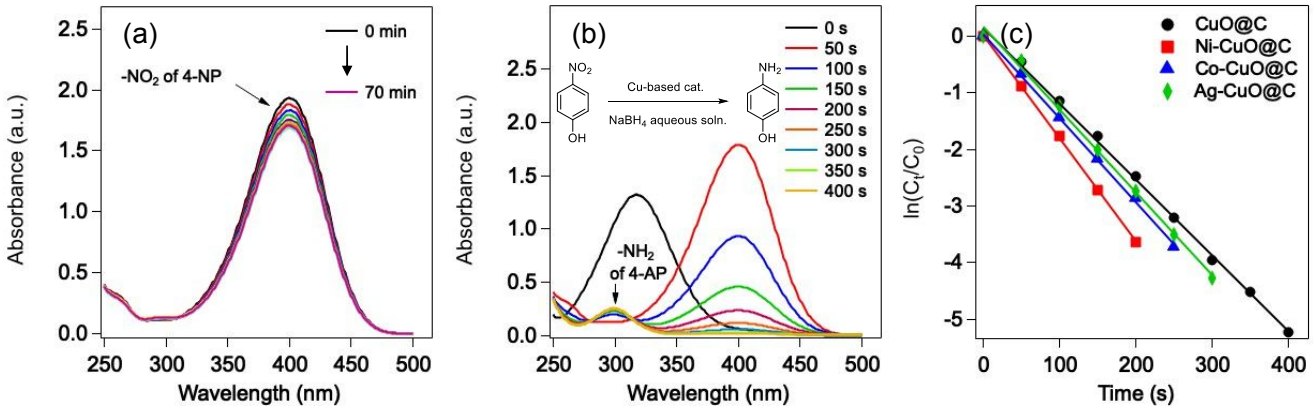

Fig. 5 Time-dependent UV-Vis absorption spectra of the 4-nitrophenol reduced by $NaBH_4$ without Cu-based catalysts (a) and with CuO@C catalyst (b), and the plots of $\ln(C_t/C_0)$ versus time at room temperature for all synthesized catalysts (c). The solid lines correspond to the best straight line fit.

Reduction of nitro-aromatic compounds

Based on the above kinetic studies, the Ni-CuO@C catalyst was selected to determine the selectivity and electronic limitations of the reaction (Fig. 6). UV-Vis absorption spectra was used to follow the catalytic reduction of several nitroaromatic compounds over Ni-CuO@C at 25 °C with identification of the final products was confirmed by GC-MS (Table S8). All nitroaromatic compounds were reduced to complete reduction. The conversion for these substituted nitro-compounds with Ni-CuO@C in the first 3 min were between 27% to >99% thereby undergoing different rates based on electronic substitution (Table S8, Fig. S15). The reaction rates and electronic sensitivity constant, ρ, were calculated and plotted but did not show a clear electronic correlation (Fig. 6).[59]

In terms of selectivity, the reduction of 1,4-dintrobenzene is fully converted to 1,4-diaminebenzene within 13.3 minutes. Bimetallic Ni-CuO@C is limited in chemoselectivity for aldehyde reduction in the presence of the nitro group. Over time the nitro-group is reduced first followed by the -CHO group leading to 4-aminobenzylalcohol as the final product. However, in the chemoselective reduction of 4-nitrobenzoic acid to 4-aminobenzoic acid, occurring in less than 1 minute, no further reduction was observed as confirmed by GC-MS. Catalytic reusability was not conducted due to the difficulty in recollection and redispersion of the catalyst. Optimization of the catalyst usability is underway.

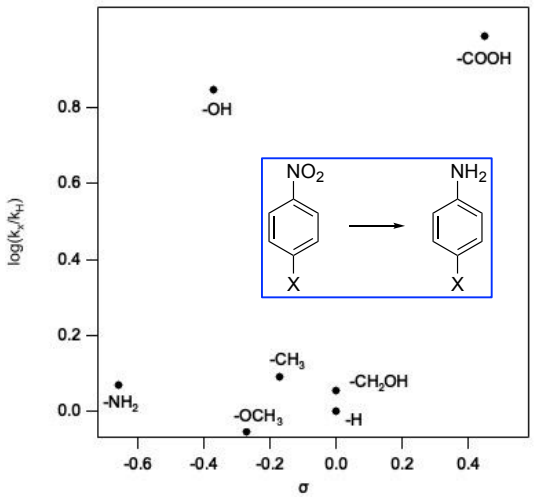

Fig. 6 The Ni-CuO@C catalyzed conversion efficiencies of the reduction reaction plotted as a Hammett plot.

Reduction of nitrobenzene in batch reaction

The catalytic activity of CuO@C under scalable conditions was conducted to compare Ni-CuO@C (entry 2) compared to CuO@C (entry 1) as shown in Table 2. The synthesized catalysts were stable during reactions since there was a negligible concentration of Cu leached into solution as tested by ICP-OES. The catalytic activity is maintained with half the Ni-CuO@C catalyst loading (entry 3) and slightly decreases to 80.7% yield even with 1 mol% catalyst (entry 4). The other synthesized bimetallic catalysts (entries 5-6) are only slightly better than the Cu monometallic catalyst but not as good as the Ni bimetallic catalyst. The turnover number (TON) of our catalysts are higher than that of similar Cu-based catalysts that others have used (entries 7-10).[60-61] We can use less catalyst while maintaining high conversion over similar times as these catalysts.

The increased activity seen in these catalysts is due to the inherent activity of copper as a good conductor. Despite the low specific surface area and the limited pore size of these catalysts there is still a significant impact for reaction enhancement. The heterogeneous catalysed reduction reaction is in line with a Langmuir Hinshelwood model with adsorption of the 4-NP and borohydride.[56,62] Hydrogen and electrons are then transferred to form 4-AP which is then desorbed from the surface. However, CuO and Cu_2O are not good conductors. The synthesis method for CuO@C creates a mixture of copper oxidation states as shown by XPS resulting in equal amounts of Cu/Cu_2O and CuO.

This journal is © The Royal Society of Chemistry 20xx

Please do not adjust margins

Table 2 Reduction of nitrobenzene in batch reaction.

Entry	Catalyst	mol % Cu	Conv. (%)[b]	TON[c]	Ref
1	CuO@C	5.0	72.9	14.6	-
2	Ni-CuO@C	5.0	100	20	-
3	Ni-CuO@C	2.5	100	40	-
4	Ni-CuO@C	1.0	80.7	80.7	-
5	Co-CuO@C	5.0	78.5	15.7	-
6	Ag-CuO@C	5.0	85.8	17.2	-
7	a-Cu@C	5.0	67.5	13.5	28
8	CuO	10.0	79	7.9	60
9	Cu NPs	10.0	98	9.8	60
10	$CuFe_2O_4$	100.0	100	1	61
11	Cu np/AC	>100.0	92-100	NA	68

[a] Reaction conditions: nitrobenzene (1 mmol), $NaBH_4$ (3 equiv.), catalyst (1-5 mol%), and THF:H_2O (1:2, 3 mL), 70 °C, 2 h.
[b] Determined by GC-MS using biphenyl as internal standard.
[c] Turnover number (TON) = [moles of converted substrate (nitrobenzene)] × (moles of Cu)$^{-1}$.

The composite of a Cu_2O-Cu-CuO has been found to be efficient and a highly active catalyst due to the transfer between the ternary copper oxidation states.[63] The MOF-derived ternary composite shows similar high activity. Nickel has been shown to increase the redox activity for Cu-Ni bimetallic nanoparticles.[64] The increased effect of Ni in combination with the ternary composite is what results in such a highly active catalyst.

The catalytic performance of the synthesized catalysts, CuO@C and M-CuO@C with M = Ni, Co, Ag, was compared to that of previously reported catalysts for the same reaction (Supporting information Table S9). In comparison with carbon supported catalysts, CuO@C performs 4-NP reduction with a higher turnover rate (6 mmol/g_{cat}/min compared to 0.01-1.04) and a higher activity factor including those supported on graphene oxide,[65] polymer-derived support,[66] and a carbon composite.[67] The Cu based catalyst on activated carbon is the only catalyst with a similar activity factor (accounts for activity normalized to catalyst mass) compared to CuO@C (tabulated data is also shown in Table 2 entry 11).[68] A comparison of the bimetallic Cu-based catalysts to similar bimetallic Cu-based catalysts synthesized by others shows that in each of the cases, M-CuO@C have much higher turnover rates, larger rate constants and activity factors (Table S9, entries 11-13).[69-71] A comparison with carbon-based supported noble metal catalysts such as gold supported on activated carbon,[72] or gold supported on CuO nanoparticles,[41] or even palladium nanoparticles supported on nanoparticles[73] reveals that the Ni-CuO@C catalyst has the higher turnover frequency, rate constant and activity factor (Table S9, entries 14-16).

Conclusions

Bimetallic Cu-based carbon supported catalysts (M-CuO@C, M = Ni, Co, and Ag) can be successfully synthesized by themolysis of HKUST-1 impregnated with a second metal and impregnated with TNT. The materials possess hierarchical porous structures (micro-, meso- and macropores) with highly dispersed copper nanoparticles. The M-CuO@C catalysts shows enhanced catalytic activity over CuO@C for reduction of 4-nitrophenol. Characterization of the materials indicates smaller particle size results from an added metal. Out of the bimetallic materials, Ni-CuO@C was the most active catalyst, which showed the highest turnover frequency of 12 mmol 4-NP·g_{cat}^{-1}·min^{-1} with full conversion within 3.3 minutes. Further studies into applications for the bimetallic Cu-based catalysts for other reductions and hydrogenation reactions are underway. The rapid decomposition of bimetallic-HKUST-1 with TNT additive is a powerful strategy that can be generalized to other commercially available MOF materials for preparing highly active heterogeneous bimetallic catalysts.

Conflicts of interest

There are no conflicts to declare.

Acknowledgements

The work was supported by the Simmons Research Endowment at Brigham Young University while the synthesis of materials was supported by the US Department of Energy [Office of Basic Energy Sciences] DE-FG02-08ER 15997 at the University of Michigan.

Notes and references

1 H. Furukawa, K. E. Cordova, M. O'Keeffe and O. M. Yaghi, *Science*, 2013, **341**, 1230444.
2 A.-L. Li, Q. Gao, J. Xu and X.-H. Bu, *Coord. Chem. Rev.*, 2017, **344**, 54–82.
3 K. K. Gangu, S. Maddila, S. B. Mukkamala and S. B. Jonnalagadda, *Inorg. Chim. Acta*, 2016, **446**, 61–74.
4 R. J. Kuppler, D. J. Timmons, Q.-R. Fang, J.-R. Li, T. A. Makal, M. D. Young, D. Yuan, D. Zhao, W. Zhuang and H.-C. Zhou, *Coord. Chem. Rev.*, 2009, **253**, 3042–3066.
5 Z. Li, F. Meng, J. Zhang, J. Xie and B. Dai, *Org. Biomol. Chem.*, 2016, **14**, 10861-10865.
6 S. Ma and H.-C. Zhou, *Chem. Commun.*, 2010, **46,** 44.
7 K. Suresh and A. J. Matzger, *Angew. Chem., Int. Ed.*, 2019, **58(47)**, 16790-16794.
8 Z. Hu, B. J. Deibert and J. Li, *Chem. Soc. Rev.*, 2014, ***43***, 5815-5840.
9 L. E. Kreno, K. Leong, O. K. Farha, M. Allendorf, R. P. Van Duyne and J. T. Hupp, *Chem. Rev.*, 2012, ***112(2)***, 1105-1125.
10 Y.-Z. Chen, R. Zhang, L. Jiao and H.-L. Jiang, *Coord. Chem. Rev.*, 2018, **362**, 1-23.
11 Q. Wang and D. Astruc, *Chem. Rev.*, 2020, **120**, 1438-1511.
12 V. L. Gemini, A. Gallego, V. M. de Oliveira, C. E. Gomez, G. P. Manfio and S. E. Korol, *Int. Biodeterior. Biodegrad.*, 2005, **55**, 103-108.
13 T.-L. Lai, K.-F. Yong, J.-W. Yu, J.-H. Chen, Y.-Y. Shu and C.-B. Wang, *J. Hazard. Mater.*, 2011, **185**, 366-372.
14 J. Li, D. Kuang, Y. Feng, F. Zhang, Z. Xu and M. Liu, *J. Hazard. Mater.*, 2012, **201**, 250-259.
15 A. Corma and P. Serna, *Science*, 2006, **313 (5785)**, 332–334.

16 K. Venkatraman, The Chemistry of Synthetic Dyes; Academic Press: New York, 1952; **Vol. I**, p 184.
17 R. Joncour, A. Ferreira, N. Duguet and M. Lemaire, *Org. Process Res. Dev.*, 2018, **22 (3)**, 312−320.
18 S. Wunder, Y. Lu, M. Albrecht and M. Ballauff, *ACS Catal.*, 2011, **1**, *8*, 908−916.
19 T. Aditya, A. Pal, and T. Pal, *Chem. Comm.*, 2015, **51**, 9410-9431.
20 Y. Wang, S. Sang, W. Zhu, L. Gao and G. Xiao, *Chemical Engineering Journal*, 2016, **299**, 104-111.
21 Y. Wang, Y. Miao, S. Li, L. Gao and G. Xiao, *Molecular Catalysis*, 2017, **436**, 128-137.
22 H. Wang, Q.-L. Zhu, R. Zou and Q. Xu, *Chem.*, 2017, **2**, 52−80.
23 M. H. Yap, K. L. Fow and G. Z. Chen, *Green Energy Environ.*, 2017, **2(3)**, 218−245.
24 J.-K. Sun and Q. Xu, *Energy Environ. Sci.*, 2014, **7**, 2071−2100.
25 B. Liu, H. Shioyama, T. Akita and Q. Xu, *J. Am. Chem. Soc.*, 2008, **130(16)**, 5390−5391.
26 H.-L. Jiang, B. Liu, Y.-Q. Lan, K. Kuratani, T. Akita, H. Shioyama, F. Zong and Q. Xu, *J. Am. Chem. Soc.*, 2011, **133(31)**, 11854−11857.
27 K. A. McDonald, N. Ko, K. Noh, J. C. Bennion, J. Kim and A. J. Matzger, *Chem. Commun.*, 2017, **53**, 7808–7811.
28 A. H. T. Nguyen-Sorenson, C. M. Anderson, S. K. Balijepalli, K. A. McDonald, A. J. Matzger and K. J. Stowers, *Inorg. Chem. Front.*, 2019, **6**, 521-526.
29 J. I. Feldblyum, M. Liu, D. W. Gidley and A. J. Matzger, *J. Am. Chem. Soc.,* 2011, **133**, 18257-18263.
30 R. Das, P. Pachfule, R. Banerjee and P. Poddar, Nanoscale 2012, 4, 591-599.
31 H. Liu, S. Zhang, Y. Liu, Z. Yang, X. Feng, X. Lu and F. Huo, *Small*, 2015, **11**, 3130–3134.
32 P. H. Zhang, Y. M. Sui, G. J. Xiao, Y. N. Wang, C. Z. Wang, B. B. Liu, G. T. Zou and B. Zou, *J. Mater. Chem. A*, 2013, **1**, 1632-1638.
33 M. Yin, C.-K. Wu, Y. Lou, C. Burda, J. T. Koberstein, Y. Zhu and S. O'brien, *J. Am. Chem. Soc.*, 2005, **127(26)**, 9506-9511.
34 F. Gul-E-Noor, B. Jee, M. Mendt, D. Himsl, A. Pöppl, M. Hartmann, J. Haase, H. Krautscheid and M. Bertmer, *J. Phys. Chem. C*, 2012, **116 (39)**, 20866-20873.
35 L. H. Wee, M. R. Lohe, N. Janssens, S. Kaskel and J. A. Martens, *J. Mater. Chem.*, 2012, **22**, 13742-13746.
36 Ö. Karahan, E. Biçer, A. Taşdemir, A. Yürüm and S. A. Gürsel, *Eur. J. Inorg. Chem.*, 2018, 1073-1079.
37 I. Kainthla, G. V. R. Babu, J. T. Bhanushali, R. S. Keri, K. S. R. Rao and B. M. Nagaraja, *New J. Chem.*, 2017, **41**, 4173-4181.
38 P. Zhang, C. Shao, Z. Zhang, M. Zhang, J. Mu, Z. Guo and Y. Liu, *Nanoscale*, 2011, **3**, 3357-3363.
39 F. Li, Y. Wang, D. Wang and F. Wei, *Carbon*, 2004, **42**, 2375-2383.
40 Y. F. Zhang, L. G. Qiu, Y. P. Yuan, Y. J. Zhu, X. Jiang and J. D. Xiao, *Appl. Catal., B*, 2014, **144**, 863–869.
41 S. Gao, X. Jia, Z. Li and Y. Chen, *J. Nanopart. Res.*, 2012, **14**, 748-758.
42 J M. C. Biesinger, L. W. M. Lau, A. R. Gerson and R. S. C. Smart, *Appl. Surf. Sci.*, 2010, **257(3)**, 887-898.
43 M. Valvo, D. Rehnlund, U. Lafont, M. Hahlin, K. Edström and L. Nyholm, *J. Mater. Chem. A*, 2014, **2**, 9574-9586.
44 K J. W. Burress, S. Gadipelli, J. Ford, J. M. Simmons, W. Zhou and T. Yildirim, *Angew. Chem., Int. Ed.*, 2010, **49**, 8902– 8904.
45 N. Mahmood, C. Zhang, H. Yin and Y. Hou, *J. Mater. Chem. A*, 2014, **2**, 15–32.
46 K. Niu, B. Yang, J. Cui, J. Jin, X. Fu, Q. Zhao and J. Zhang, *J. Power Sources*, 2013, **243**, 65–71.
47 D. A. Bulushev, A. L. Chuvilin, V. I. Sobolev, S. G. Stolyarova, Y. V. Shubin, I. P. Asanov, A. V. Ishchenko, G. Magnani, M. Riccò, A. V. Okotrub and L. G. Bulusheva, *J. Mater. Chem. A*, 2017, **5**, 10574–10583.
48 A. S. Hall, A. Kondo, K. Maeda and T. E. Mallouk, *J. Am. Chem. Soc.*, 2013, **135(44)**, 16276–16279.
49 F. Pang, F. Song, Q. Zhang, Y. Tan and Y. Han, *Chem. Eng. J.*, 2016, **293**, 129–138.
50 P. K. Chu and L. Li, *Mater. Chem. Phys.*, 2006, **96**, 253-277.
51 A. C. Ferrari and J. Robertson, *Phys. Rev. B*, 2000, **61(20)**, 14095-14107.
52 A. Sadezky, H. Muckenhuber, H. Grothe, R. Niessner and U. Pöschl, *Carbon*, 2005, **43(8)**, 1731-1742.
53 C. T. J. Low, F. C. Walsh, M. H. Chakrabarti, M. A. Hashim and M. A. Hussain, *Carbon*, 2013, **54**, 1-21.
54 A. K. Díaz-Duran and F. Roncaroli, *Electrochim. Acta*, 2017, **251**, 638-650.
55 N. Pradhan, A. Pal and T. Pal, *Langmuir*, 2001, **17(5)**, 1800-1802.
56 S. Saha, A. Pal, S. Kundu, S. Basu, T. Pal *Langmuir*, 2010, **26(4),** 2885-2893.
57 S. Gao, Y. Tang, L. Wang, L. Liu, D. Jia, Z. Zhao, J. Alloys Compd, 2017, **702**, 531-537.
58 H. Yen, Y. Seo, S. Kaliaguine and F. Kleitz, *ACS Catal.*, 2015, **5**, 5505-5511.
59 E. V. Anslyn and D. A. Dougherty, Modern Physical Organic Chemistry; University Science Book: Sausalito, California, 2006.
60 Z. Duan, G. Ma and W. Zhang, *Bull. Korean Chem. Soc.*, 2012, **33(12)**, 4003-4006.
61 B. Zeynizadeh, F. M. Aminzadeh and H. Mousavi, *Res. Chem. Intermed.*, 2019, **45**, 3329-3357.
62 P. Herve, M. Perez-Lorenzo, L. M. Liz-Marzan, J. Dzubiella, Y. Lubc and M. Ballauff, *Chem. Soc. Rev*., 2012, **41**, 5577-5587.
63 A. K. Sasmal, S. Dutta, and T. Pal. *Dalton Trans.,* 2016, **45**, 3139-3150.
64 S. Vivek, S. Preethi, T. H. V. Kumar, A. K. Sundarmoorthy, K. S. Babu*, J. Alloys Compd*. 2020, **816**, 152608-152618.
65 T. Wu, M. Chen, L. Zhang, X. Xu, Y. Liu, J. Yan, W. Wang and J. Gao, *J. Mater. Chem. A*, 2013, **1**, 7612-7621.
66 A. N. Imangaliyeva, Y. Mastai and G. A. Seilkhanova, *J. Nanopart. Res.*, 2019, **21(97)**, 1-11.
67 S. B. Khan, F. Ali and K. Akhtar, *Carbohydr. Polym.*, 2019, **207**, 650-662.
68 S. Wang, S. Gao, Y. Tang, L. Wang, D. Jia and L. Liu, *J. Solid State Chem.*, 2018, **260**, 117-123.
69 F. Ali, S. B. Khan, T. Kamal, Y. Anwar, K. A. Alamry and A. M. Asiri, *Chemosphere*, 2017, **188**, 588-598.
70 J. Yang, X. Shen, Z. Ji, H. Zhou, G. Zhu and K. Chen, *Appl. Surf. Sci.*, 2014, **316**, 575–581.
71 A. D. Verma, S. Pal, P. Verma, V. Srivastava, R. K. Mandal and I. Sinha, *J. Environ. Chem. Eng.*, 2017, **5**, 6148–6155.
72 A. Kumar, M. Belwal, R. R. Maurya, V. Mohan and V. Vishwanathan, *Materials Science for Energy Technologies*, 2019, **2**, 526-531.
73 T. Baran, *Catal. Lett.*, 201**9**, **149**, 1721-1729.

This journal is © The Royal Society of Chemistry 20xx

Please do not adjust margins

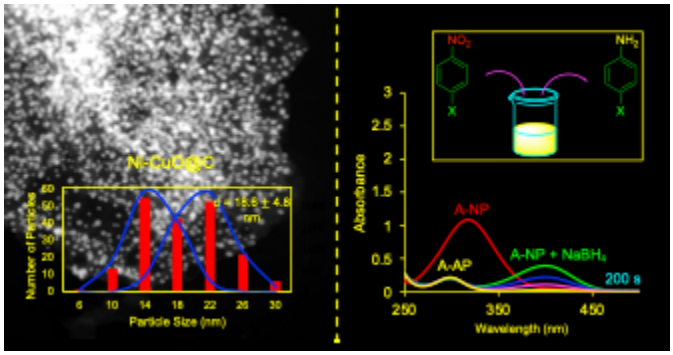
Number of Particles
Particle Size (nm)
Absorbance
Wavelength (nm)
A-NP
A-AP
A-NP + NaBH4
200 s